Hindawi
Advances in Civil Engineering
Volume 2022, Article ID 6232757, 18 pages
https://doi.org/10.1155/2022/6232757

Research Article

Behavior of Steel-Fiber-Reinforced Concrete (SFRC) Slab-on-Grade under Impact Loading

Essetemariam Tekleab and Temesgen Wondimu

Department of Civil Engineering, Addis Ababa Science and Technology University, Addis Ababa, Ethiopia

Correspondence should be addressed to Temesgen Wondimu; temesgen.wondimu@aastu.edu.et

Received 13 February 2022; Revised 24 March 2022; Accepted 8 April 2022; Published 19 May 2022

Academic Editor: Raizal Saifulnaz Muhammad Rashid

Structures such as industrial pavements, roads, parking areas, and airport runways are often slab-on-grade where steel-fiber reinforcement can substitute conventional steel reinforcement. Due to the dynamic nature of loading while in service, these structures are exposed to the damaging effects of impact loading, such as strength and stiffness deterioration in materials or structural elements. In this study, the behavior of concrete slab-on-grade with steel-fiber-reinforced concrete under impact load has been investigated by considering different parameters. Nonlinear finite element software ABAQUS/Explicit is used to simulate the system. The accuracy of the nonlinear finite element models is verified using experimental work available in the literature. A total of 108 specimens are simulated by varying the volume fraction of steel fiber by 0.5%, 1%, and 1.5% coupling with the impact mass and velocity from the control specimen and variation of load location, thickness, and aspect ratio. The analysis results revealed that the addition of 0.5%, 1%, and 1.5% volume fraction of steel fiber in concrete could effectively accommodate up to 0%, 10%, and 26% reduction of thickness, respectively. These results confirmed that the appropriate use of steel fiber in concrete can be a feasible solution to improve the overall performance of slab-on-grade. Moreover, an increase in the aspect ratio of steel fiber improves the crack resistance of steel-fiber-reinforced concrete slab-on-grade, but a further increase in aspect ratio reduces the performance due to local crushing of concrete.

1. Introduction

Reinforced concrete structures subjected to dynamic loadings, such as industrial pavements, roads, parking areas, and airport runways, are often called slab-on-grade, which necessitate the consideration of dynamic load effect for design. Most studies have been conducted to assess the dynamic loading of vehicle response to pavements. Nevertheless, pavements in airports, container terminals, logistics terminals, storage areas, industrial areas, parking lots, areas operated by falling objects or special machinery, etc. are subjected to long-term static or impact loading [1]. A local effect resulting from such impact loading leads to different resistance mechanisms than those activated in quasistatic conditions because of wave propagation, mobilization of inertial forces, and changes in strain rates of material properties.

Concrete is a heterogeneous and brittle material, and the progression of a crack occurs within the material, leading to its degradation under dynamic loading. Consequently, the structural degradation of runway pavement is triggered by deflection and cracking, and the dynamic stiffness of the distressed runway pavement is reduced exponentially with the age of the runway pavement due to repetitive incidents. In addition, the high speed and heavily weighted aircrafts exert huge contact pressure on the runway pavement during the take-off and after the landing of aircrafts frequently. As a consequence, surface depression, rutting, and potholes are often visible for heavily serviced runway pavements or severe damage after accidents [2–6]. The potential exists to improve the dynamic load performance of concrete at the structural level with the advent of steel-fiber-reinforced concrete (SFRC), which is a composite material in which steel fibers are homogeneously mixed in plain concrete, compared to members of conventional concrete structures.

Steel-fiber-reinforced concrete is regarded as a fiber strengthening system. The experimental tests investigated at

Table 1: Material parameters of plain and fiber-reinforced concrete [57].

Material parameter	Plain concrete	Fiber-reinforced concrete		
		0.5% V_f	1% V_f	1.5% V_f
Average compressive strength (N/mm^2)	50	48	48.6	50.7
Average split tensile strength (N/mm^2)	4.02	4.59	4.09	4.05
Young's modulus (N/mm^2)	37440	26660	25500	25300

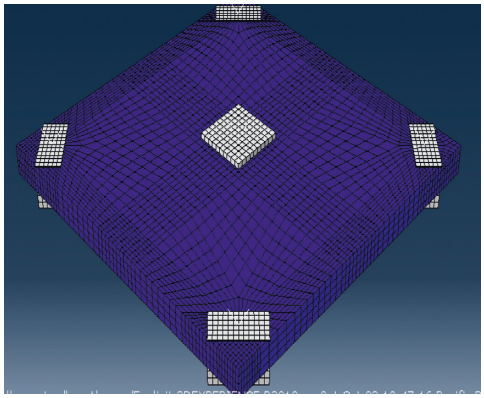

Figure 1: Modeled specimens for validation.

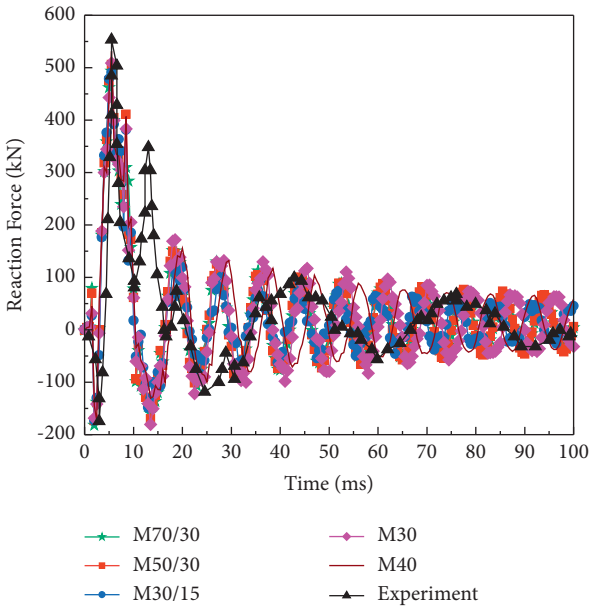

Figure 2: Mesh sensitivity study.

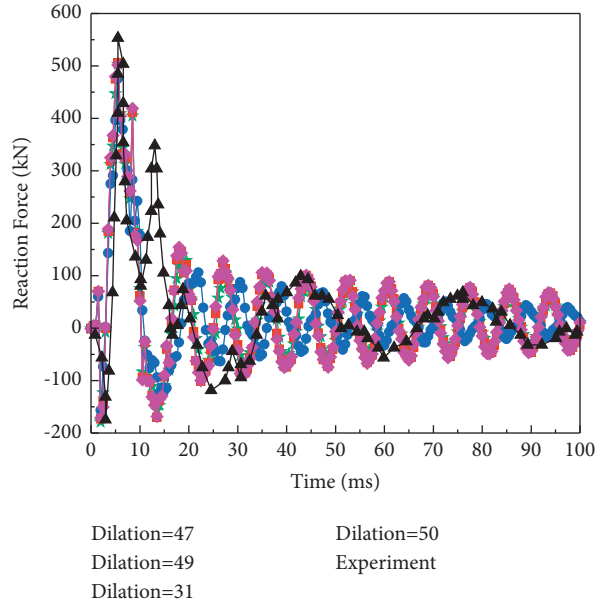

Figure 3: Effect of dilation angle for 0% fiber (TH21) specimen.

the material level demonstrated that steel fibers improved the resistance to crack growth, reduced deflection, and increased the fatigue life and impact resistance of plain concrete under different loads. The inclusion of steel fibers in concrete can greatly enhance static flexural strength, impact strength, shear and torsional strength, direct tensile strength, fatigue strength, impact resistance, ductility, and failure toughness [7–9]. The most substantial advantage of adding fibers to concrete is the improvement in impact resistance [10–17]. Concrete strengthened with different kinds of fibers withstood explosives, dropped weights, and dynamic bending, tensile, and compressive loads with three to ten times the dynamic strength of ordinary concrete [18]. According to ACI 544 4R, steel-fiber-reinforced concrete beams have a total energy absorption capacity of 40 to 100 times that of unreinforced beams.

Several researchers have investigated the behavior of steel-fiber-reinforced concrete (SFRC) slab-on-grade under monotonic loading [19–31]. However, the studies focusing on slab-on-grade under the impact are limited.

It is, therefore, necessary to evaluate the impact resistance of the conventional runway concrete pavement and improve its performance by adding steel fiber. Steel-fiber-reinforced concrete is an impact-resistant material that has demonstrated favorable energy dissipation and ductility properties via the progression of impact toughness and tensile strength. Due to the lack of sufficient data on the dynamic properties of steel-fiber-reinforced concrete in previous investigations, the design procedures and analysis of SFRC are not well developed.

In this study, the behavior of slab-on-grade under impact load has been investigated. The use of steel-fiber-reinforced concrete in reducing the thickness of the slab is examined, and the influence of load location on steel-fiber-reinforced concrete slab-on-grade under impact loading is explored. Nonlinear finite element analysis with a damaged plasticity model for both normal concrete and steel-fiber-reinforced concrete in ABAQUS/Explicit is used to simulate the slabs.

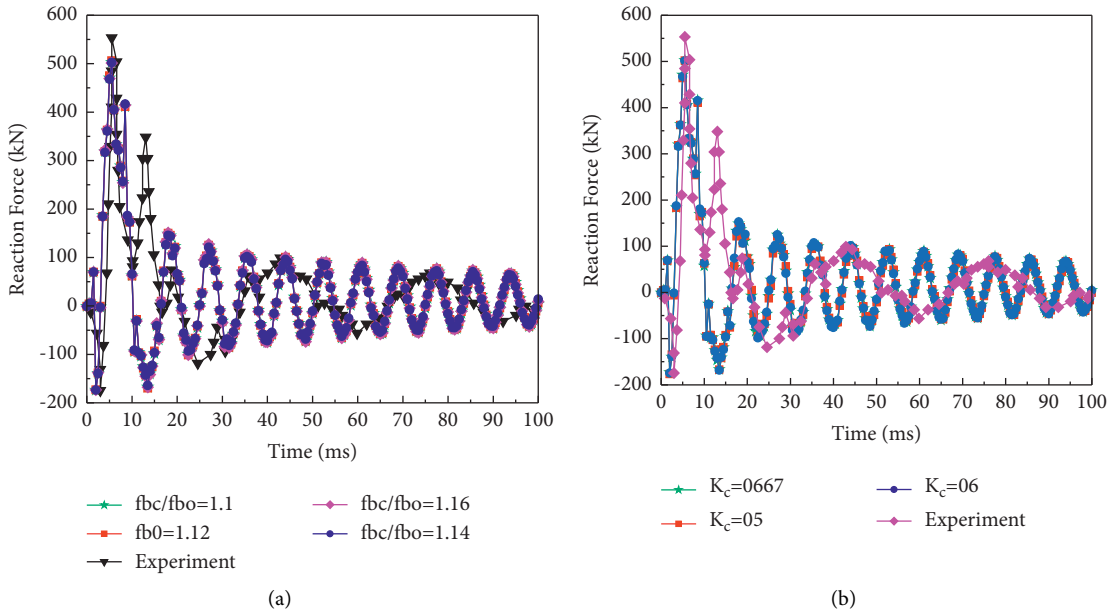

Figure 4: Calibration for CDP parameters. (a) Effect of stress ratio for 0% fiber (TH21) specimen. (b) Effect of shape factor for 0% fiber (TH21) specimen.

The accuracy of the nonlinear finite element models is verified using experimental results conducted by other researchers. Then, the slab cross section and the material used for slab-on-grade are selected from the validated specimens for a control specimen. A total of one hundred eight specimens are simulated by using the volume fraction of steel fiber of 0.5%, 1%, and 1.5% coupling with the mass and velocity from the control specimen and variation of load location, thickness, and aspect ratio.

2. Materials and Methods

2.1. Finite Element Discretization. All finite element models are developed with the commercial finite element software ABAQUS. This software offers an advantage in that the models can be easily used and customized by other researchers or pavement engineers, which will benefit the applicability of the proposed methodology for different boundary conditions, pavement geometry, and material properties.

In this research, to model the concrete slab, subgrade, and supporting plate, a 3-D eight-node reduced integration with enhanced hourglass control brick element (C3D8R) is used in all the modeling. Two-node linear three-dimensional truss elements (T3D2) having three degrees of freedom in each node were used to model steel reinforcements. And for the impactor, the discrete rigid element is used. The ABAQUS/Explicit element libraries are used for the analysis.

In this study, the embedded method of interaction is adopted between the concrete and the reinforcement bars so that perfect bond and displacement continuity are achieved between concrete and steel. The interaction between concrete and reinforcement after cracking, such as bond-slip was incorporated only in a simplified way using the tension stiffening in the concrete model, is adopted to approximately simulate load transfer across cracks through the reinforcement bars [32–34].

General surface to surface contact interaction was used to define the contact between drop-weight and the specimen, the specimen and the supporting systems, and concrete slab and subgrade. For the purpose of defining the pressure behavior of the contact interaction in the normal direction, hard contact is used. The hard contact relationship does not permit the tensile stress transfer across the interface. The friction across distinct parts of the contact is simulated using an isotropic penalized friction formulation. A friction coefficient of 0.30 is selected to define the friction between the top support steel plates and the concrete specimen [35], and a friction coefficient of 0.60 is selected to define the friction between the bottom support steel plates and the concrete specimen. For the contact between concrete slab and subgrade, a friction coefficient of 0.5 is selected. The drop-weight is modeled in an initial position close to the specimen surface (10 mm offset) with a predefined velocity equal to that taken from experimental data. The gravitational acceleration is applied to both the drop-weight and the specimen to simulate gravitational effects.

The slab is restrained in x, y, and z directions at the bottom and in the y direction only at the top. To imitate experimental conditions and avoid untimely localized failure, steel plates of 50 mm thickness for the bottom and 10 mm thickness for the top were added at the supporting points.

The subgrade is idealized as an elastic solid. To predict the pavement response to a vertical impact load, the bottom of the model was fully fixed, and rollers on the sides of the model allowed free vertical deformation.

2.1.1. Material Models. The concrete damage plasticity model (CDPM) was used in this research for modeling

Table 2: Summary of input parameters adopted in the CDP model.

Plasticity parameters	Th21 (0% vf)	Model based on steel fiber content		
		Th31 (0.5% vf)	Th41 (1% vf)	Th51 (1.5% vf)
Dilation angle (ψ) (calibrated)	49°	31°	45°	49°
Shape factor (Kc) (calibrated)	0.64	0.6	0.5	0.6
Viscosity parameter (μ)	0.0001	0.0001	0.0001	0.0001
Stress ratio (calibrated)	1.12	1.14	1.11	1.16
Eccentricity (ε) (default)	0.1	0.1	0.1	0.1

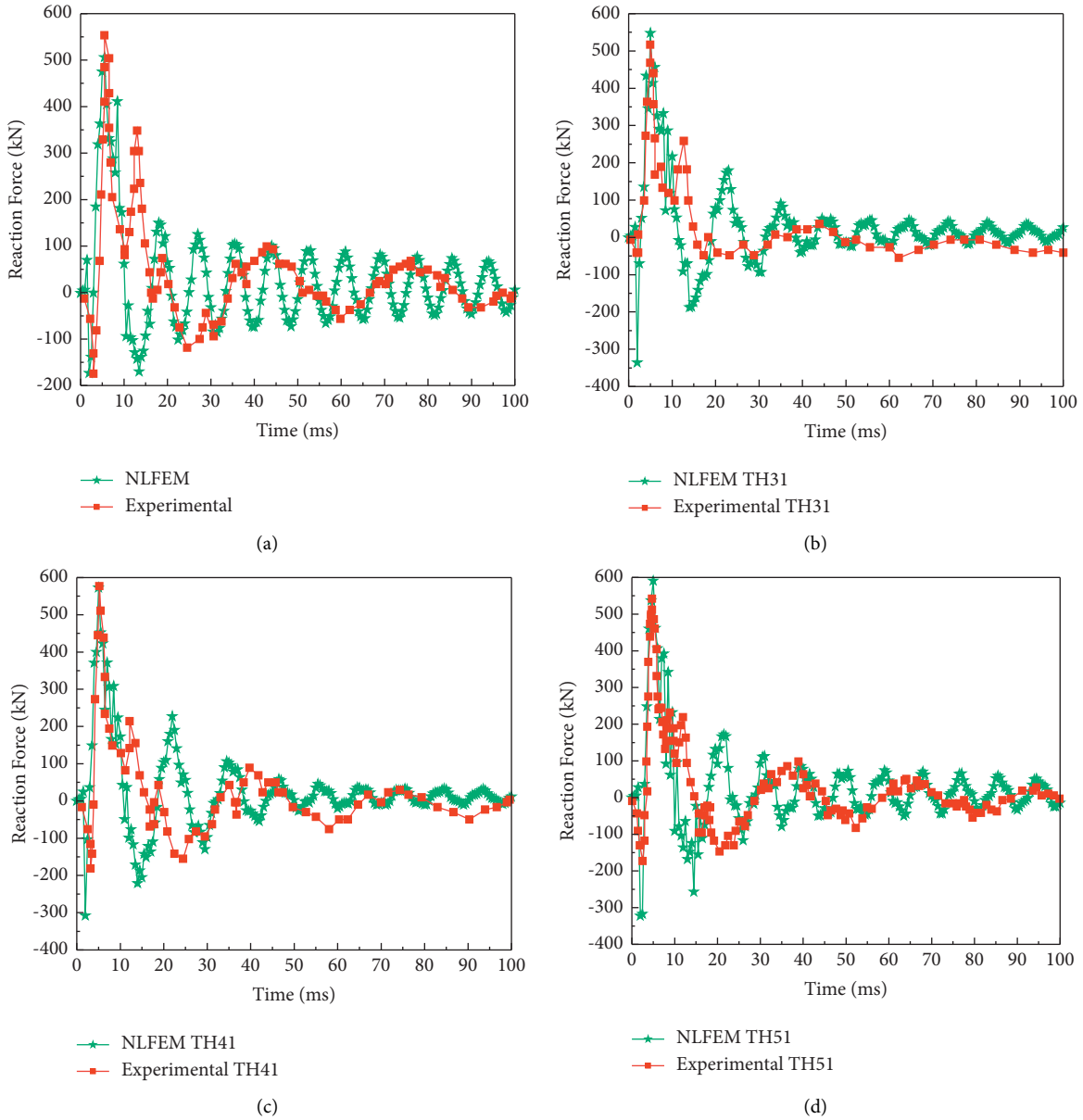

Figure 5: Reaction force vs. time history of reinforced concrete slab: (a) $V_f = 0\%$ (TH21) specimen, (b) $V_f = 0.5\%$ (TH31) specimen, (c) $V_f = 1\%$ (TH41) specimen, and (d) $V_f = 1.5\%$ (TH51) specimen.

concrete material since it utilizes the concept of isotropic damage elasticity in combination with isotropic tensile and compressive plasticity to denote the inelastic concrete behavior. Furthermore, it can be employed for ordinary concrete and is designed for applications where concrete is loaded monotonically, cyclically, and/or dynamically at low confining pressures. It comprises a composite of uncorrelated multihardening plasticity and isotropic damaged

Table 3: Comparisons of NLFEA prediction with the test results of the specimens.

Specimen	Reaction force (kN)		Variation		Peak displacement (mm)		Variation	
	NLFEM	Tet	Error	*M*%	NLFEM	Test	Error	*M*%
Th21 (vf 0%)	506.05	552	8.3%	92%	12.5	13.2	5.3%	94.7%
Th31 (vf 0.5%)	547.7	526	4.1%	96%	12	—		
Th41 (vf 1%)	582.1	591	1.5%	98.5%	11.25	13.5	15%	84%
Th31 (vf 1.5%)	590	542	8.8%	92%	10.6	12.56	15.6%	85%

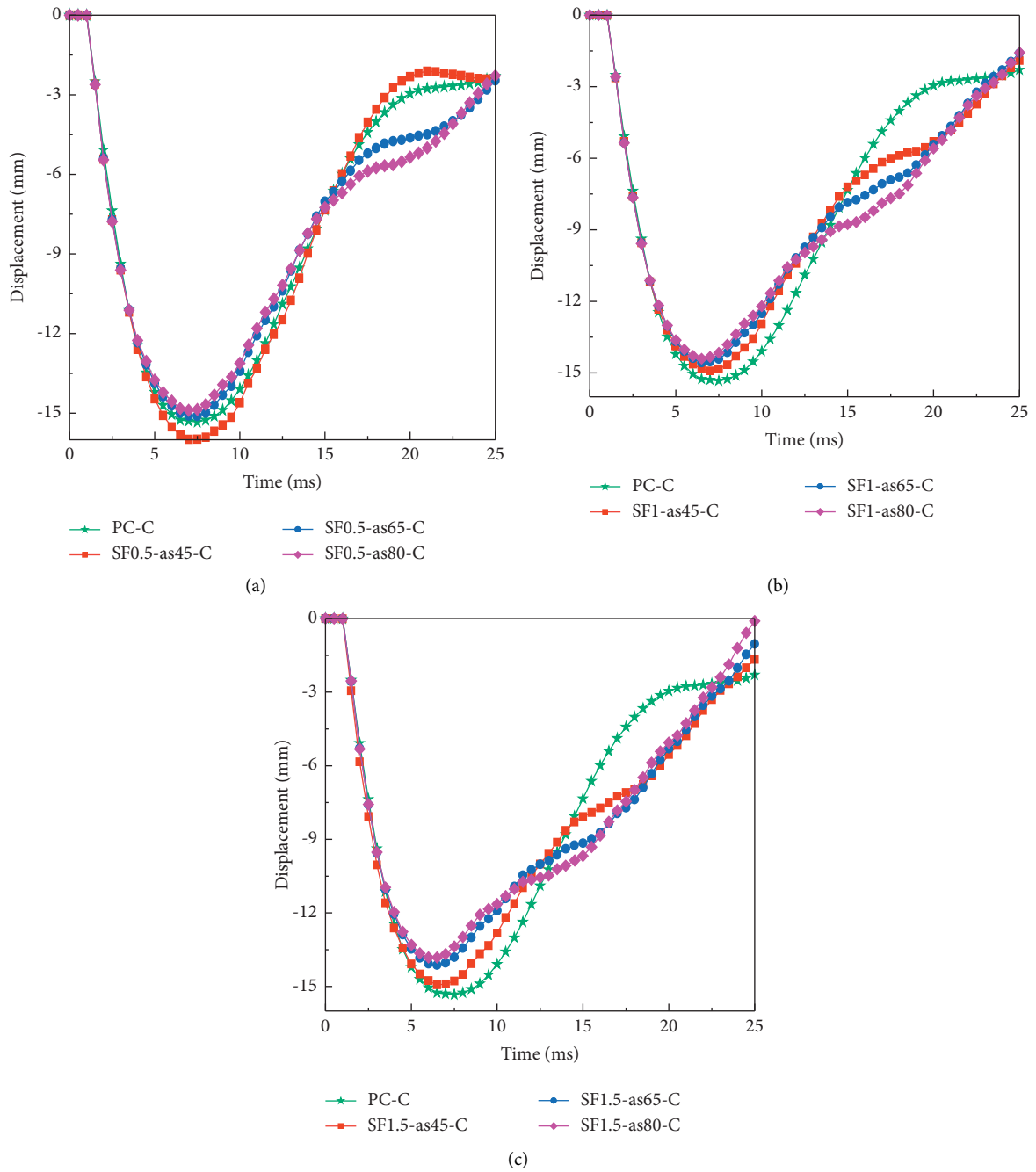

Figure 6: Displacement vs. time history response of part I specimen for center load: (a) $V_f = 0.5\%$, (b) $V_f = 1\%$, and (c) $V_f = 1.5\%$.

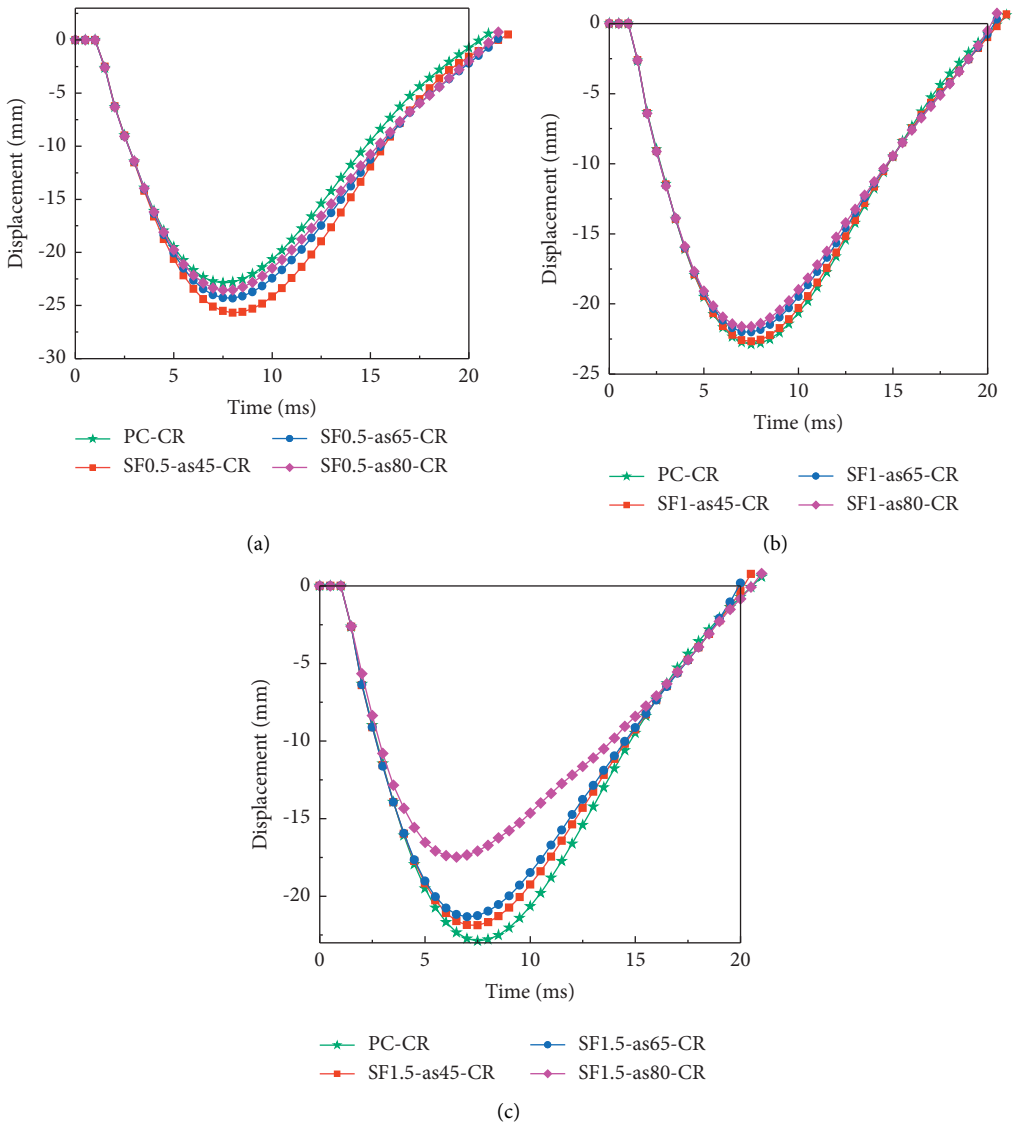

Figure 7: Displacement vs. time history response of part I specimen for corner load: (a) $V_f = 0.5\%$, (b) $V_f = 1\%$, and (c) $V_f = 1.5\%$.

elasticity to characterize the irreversible damage that occurs during fracture and permits the user to control the rigidity recovery effect during cyclic load reversal.

The uniaxial compressive and tensile stress-strain relationship for concrete is determined by the model proposed by [36] for compressive behavior and [37] for tensile behavior as they give a close result with the experimental value. The behavior of the concrete was assumed to be linear elastic up to reaching stress equal to $0.4\,f\acute{C}$. Poisson's ratio and normal weight of concrete were taken from experiments and taken to be 0.2 and 2400 kg/m^3, respectively.

In this research, the model developed by [38] is used to represent the prepeak and postpeak compressive behavior of steel-fiber-reinforced concrete (SFRC) after trying different models proposed by other researchers [39–45]. For determining the SFRC, behavior in tension constitutive stress-strain relationship given by [46] is used after trying models by [45–51] since the model by [46] gives a close result with the experimental value.

The subgrade dimension is unlimited; however, modeling the whole subgrade in a FE model is not possible. As a result, either infinite elements must be used or enough depth of soil must be modeled beyond which the results would not change [52, 53]. In this study, a Poisson's ratio of 0.3 and a subgrade depth of 10 m gave rational results, as models at more than 10 m height gave the same results, and reduction of the modeled soil depth further would yield substantial changes in the slab deflections.

An elastic-plastic model with von Mises yield criteria and isotropic hardening criteria was used to simulate the plastic behavior of the steel. The elastic-plastic model is defined by defining the elastic properties, which are the modulus of elasticity and Poisson's ratio, and the plastic part is defined using the stress-strain values. In the plastic region, the stresses and strains should be converted to the true values rather than nominal (measured) values.

The plate having elastic material behavior of Young's modulus 200 GPa and Poisson's ratio of 0.3 was employed at

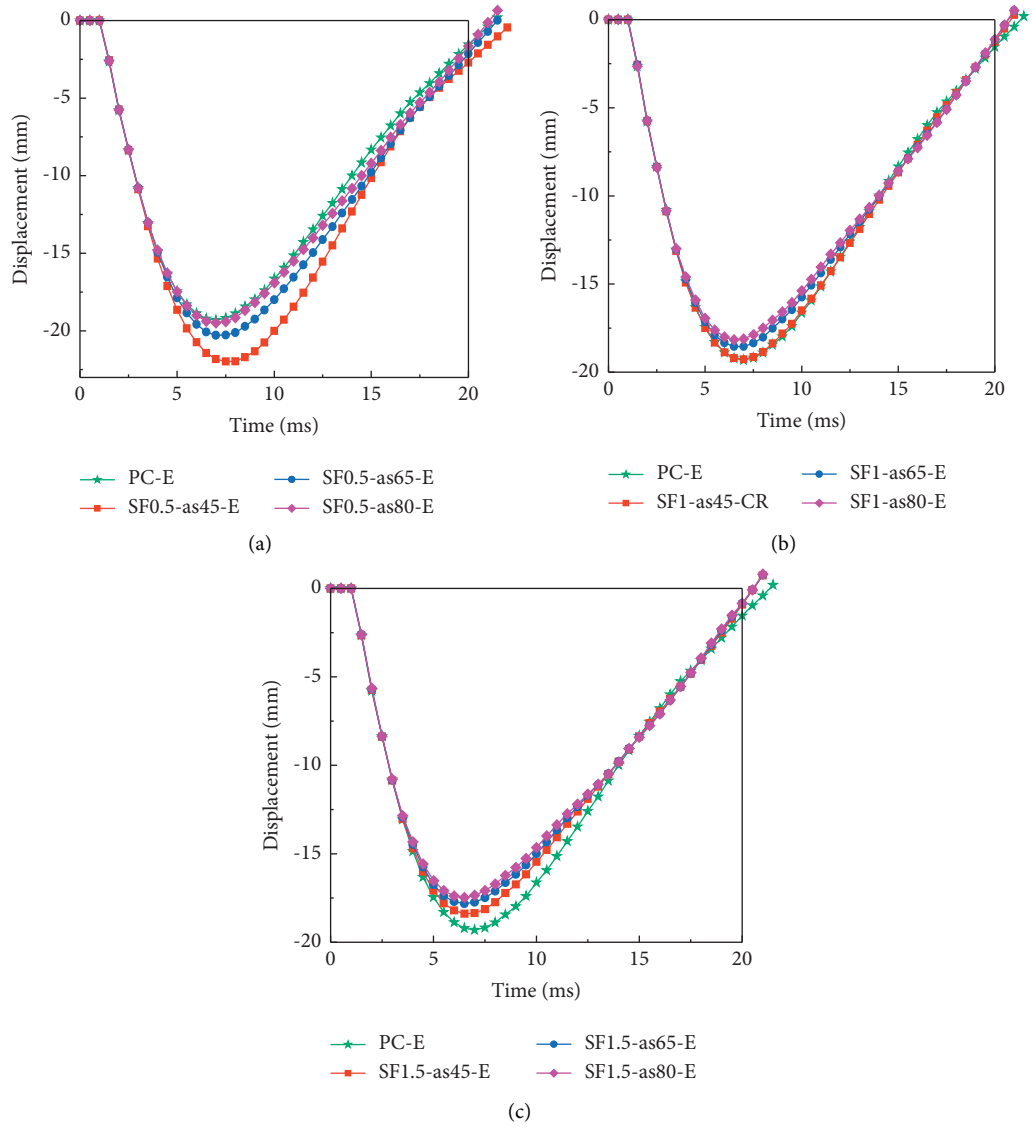

Figure 8: Displacement vs. time history response of part I specimen for edge load: (a) $V_f = 0.5\%$, (b) $V_f = 1\%$, and (c) $V_f = 1.5\%$.

this point of loading to avoid stress concentration on the concrete and premature failure or cracking of the support point to avoid premature failure of the plate.

Many research have shown that mechanical behavior of structural materials are affected by the rate of loading. Experimental studies shown that materials exhibited higher resistance to compression when tested at high strain rates. A number of equations have been proposed to to model the increase in strength of materials by what is commonly called dynamic increase factor (DIF).

There have been a number of models presented to compute strain-rate-related DIFs for plain concrete, steel-fiber-reinforced concrete, and steel reinforcement. Provisions of the fib code [54] (fib MC 2010) were used to compute DIFs for concrete, while the model proposed by [55] was used for steel reinforcement, and the model proposed by [56] was used to compute DIFs for steel-fiber-reinforced concrete. The initial selection of these models was mainly based on most investigators who considered these strain rate relationships and used the relevant modeling approach in the analysis of RC beams, columns, and frames under different dynamic loading conditions.

In applying the rate-dependent modifications, the strain rate, $10\ s^{-1}$, is used as given by [57] computed in each of the three principal stress directions of the concrete and in the direction of each of the steel reinforcing bar components.

2.2. Validation of the FEM. The finite element model developed in this paper is verified against experimental work done by [57] on the impact load behavior of SFRC.

In the experimental study, a 1800 mm × 1800 mm × 130 mm slab was simply supported on four top edges. The measured strength of the concrete was 50 MPa. The steel bars of 8 mm diameter were arranged at a spacing of 130 mm in both directions. The net thickness of the concrete overlay was

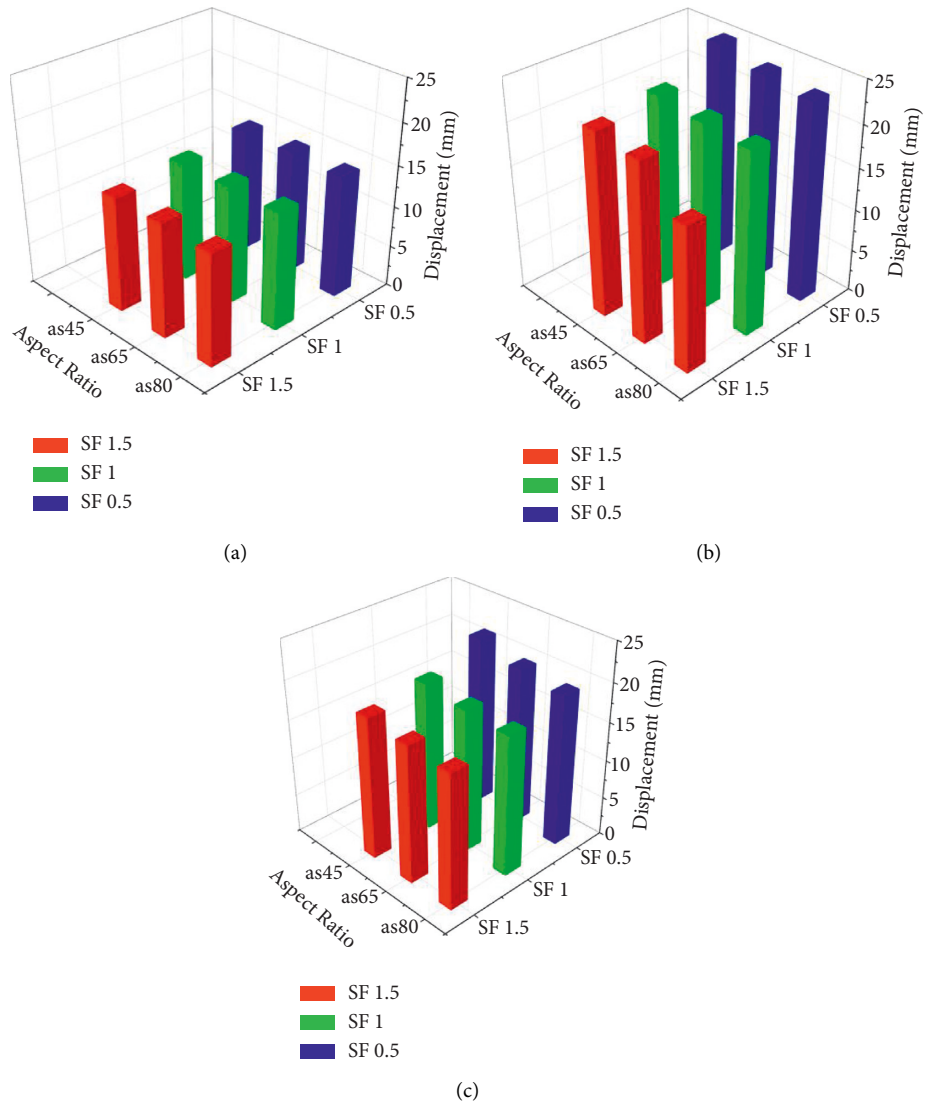

Figure 9: Combined effect of aspect ratio and fiber volume percentage (a) for center load, (b) for corner load, and (c) for edge load.

15 mm. The reinforcement bars were placed at the bottom and top of the floor slab. The experimental yield and ultimate strengths of the reinforcement bars were 414 and 475 MPa, respectively. The material properties are summarized in Table 1. In the simulations, these details were kept consistent with those in the experiments. Figure 1 shows the geometry of the specimen considered, after meshing.

The R/FRC slabs were constructed using end-hooked steel fibers with the following nominal properties: fiber length of 30 mm (1.18 in.), the diameter of 0.37 mm (0.015 in.), the aspect ratio of 80, and ultimate tensile strength of 2300 MPa as given by Hrynyk & Vecchio [57].

The hammer's striking surface consists of a 25 mm (1 in.) thick and 300 mm (11.8 in.) square steel plate with a flat contact surface. The contact surface of the drop hammer impacted the floor plate directly, producing a hard impact loading condition. Under continuous impact with increasing mass, the plate was impacted with constant impact velocity. An impact mass drop height of 3.26 m (10.7 ft) from the top surface of the slab was set, yielding a nominal impact velocity of 8.0 m/s (26.2 ft/s), which was verified by high-speed photography. A common loading protocol was endured by the slab, including successive impact events with mass levels varying from 150 to 300 kg (331 to 660 lb) [57].

Using the constitutive models discussed above, a set of analyses were carried out to choose and calibrate the most suitable SFRC constitutive model to be adopted in the subsequent parametric studies. Hence, the effects of input parameters such as mesh size, dilation angle, and viscosity parameter in constitutive equations of the damaged plasticity model have been evaluated.

2.2.1. Mesh Sensitivity. In order to perform mesh size sensitivity of the finite element model, specimen with different mesh sizes is modeled, and the result is compared as shown in Figure 2. Note that M70/30 represents a slab with mesh size of 70 mm with refined mesh size of 30 mm around

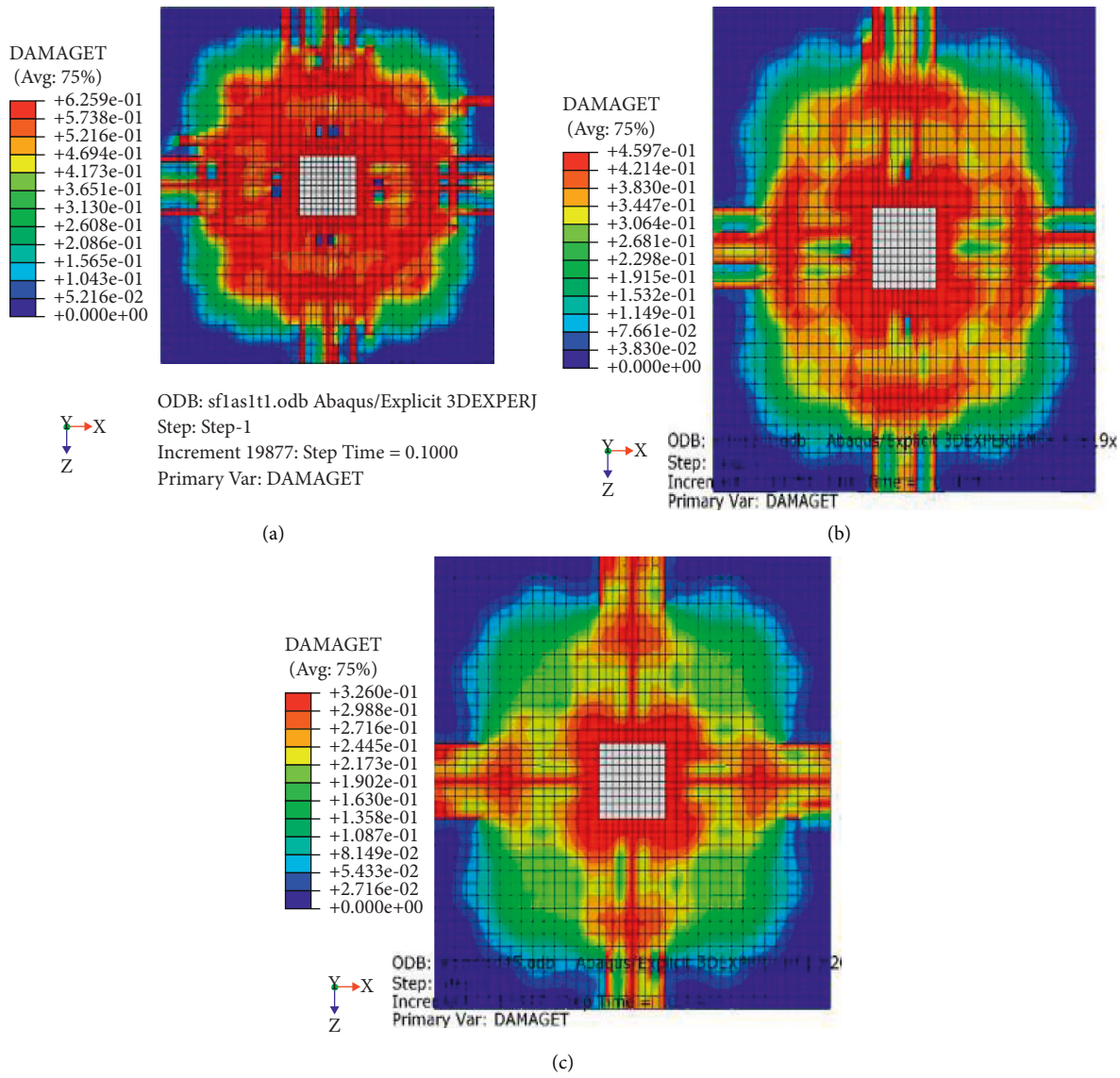

Figure 10: Tension damage of SF1-C specimens for aspect ratio of (a) as = 45, (b) as = 65, and (c) as = 80.

supporting and loading regions. It is found that a mesh size of 50 mm for the slab with 30 mm refined mesh around supporting and loading regions gives reliable results in comparison to the test result.

2.2.2. Dilation Angle (ψ). In CDP, the change in volume of the quasibrittle materials under compression (i.e., dilatancy) is modeled by assigning a dilation angle value (ψ). The dilatancy of concrete material characterizes the existence of expansion in volume when the material is exposed to triaxial stress and the consequent inelastic strain [58]. The default value of the dilation angle is 31°. Allowable values of the dilation angle are between 0° and 56° [58]. For the present study, different values of dilation angles are taken for examination.

As can be seen in Figure 3, the model response is highly influenced by the value of the dilation angle, and a dilation angle value of 49° can reasonably capture the response. Therefore, the dilation angle was chosen to be set as 49° for TH21 (reinforced concrete slab) simulations. For the other models with fiber percentages of 0.5%, 1%, and 1.5%, calibration is made for each model to take values of dilation angle which gives a closed result compared with the experimental results for each model.

2.2.3. Shape Factor of the Yield Surface ($\mathbf{K}_c$) *and Stress Ratio.* The parameter K_c is essential to define the shape of the yield surface and ranges between 0.5 and 1, and its default value is 0.667 [34]. The biaxial stress ratio ranges from 1.1 to 1.16, and its default value is 1.16. In the present study, different values of K_c with different values of *fbc/fbo* are taken for examination. As can be seen in Figure 4, the influence of K_c and *fbc/fbo* on the result of the model is significant. It can be seen that the value of $K_c = 0.64$ and *fbc/fbo* = 1.12 gives close result compared with the experimental ones. Thus, for model with 0% steel fiber volume, the parameters $K_c = 0.64$ and *fbc/fbo* = 1.12 are adopted. For the other models with fiber percentage of

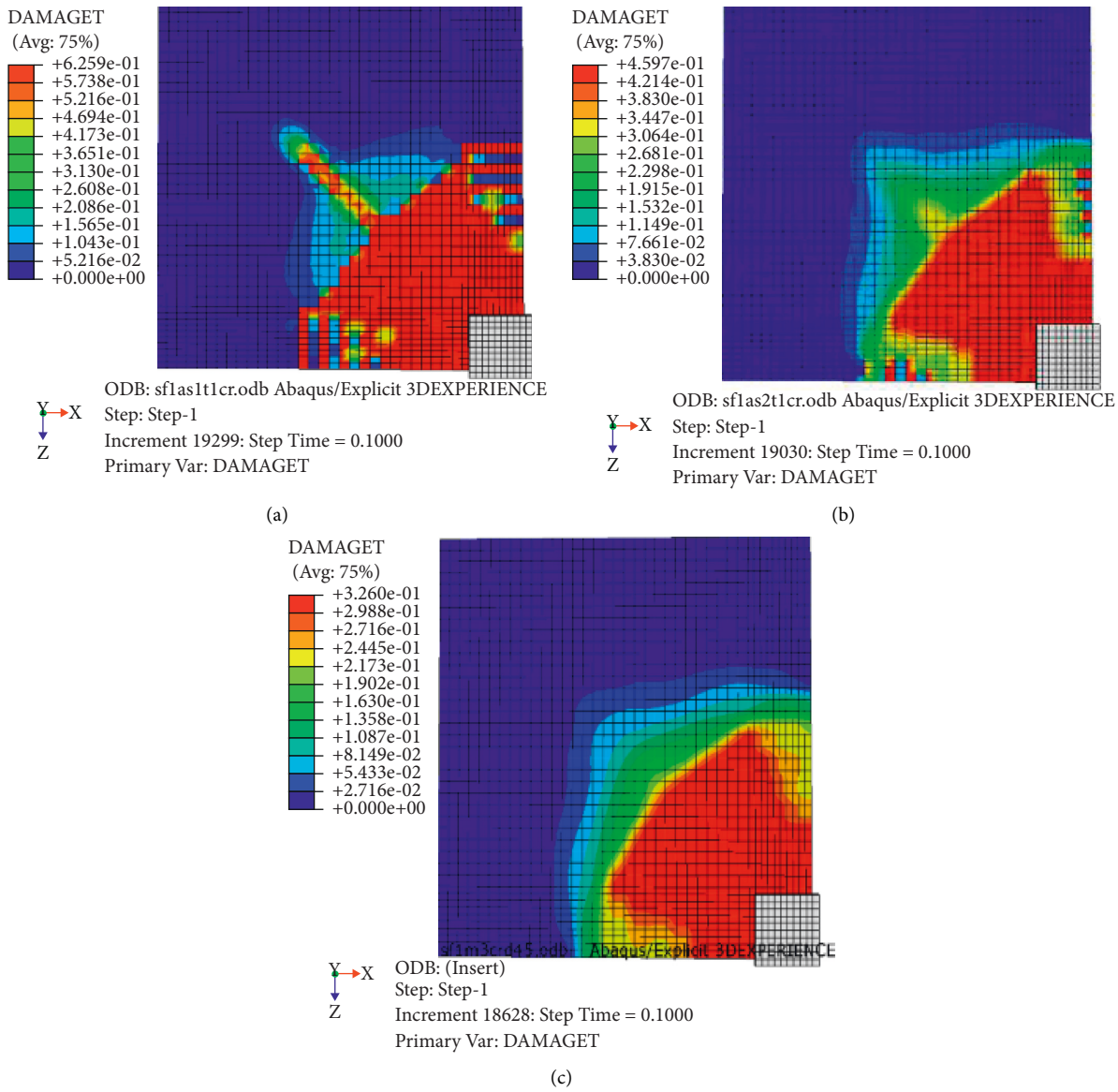

Figure 11: Tension damage of SF1-CR specimens for aspect ratio of (a) as = 45, (b) as = 65, and (c) as = 80.

0.5%, 1%, and 1.5%, calibration is made for each model to take values of K_c and *fbc/fbo* which gives close result compared with the experimental results for each model.

In general, all of the studied parameters, the mesh size, dilation angle (ψ), and the shape factor of the yield surface (K_c), are found to be critical for accurate modeling when using the concrete damaged plasticity (CDP) model. Specifically, the use of a larger mesh size can significantly reduce the computational time, but it significantly affects the accuracy of the finite element results. The values adopted in this study are summarized in Table 2.

The reaction force vs. time history curve obtained by the finite element calculations was compared with those obtained from the experimental results conducted by [57], as shown in Figure 5.

The error and overall model accuracy predicted by NLFEA of the four specimens are compared with the test result and presented in Table 3. In order to describe the overall model accuracy, and associated average underestimation or overestimation of the NLFEA, the error (%) and mean model accuracy (M (%)) were evaluated based on the relation given in Behnam et al. [59] and defined as

$$\text{Error}\,(\%) = \left|\frac{NLFEA\ \text{result} - \text{Test result}}{\text{Test result}}\right| \times 100,$$

$$\text{Mean mode accuray}, M\,(\%) = \frac{NLFEA\ \text{result}}{\text{Tesst result}} \times 100. \tag{1}$$

The comparison between the simulated and tested reaction force-time curves and midpoint displacement curve of the slab is illustrated in Figure 6. Although there exist slight discrepancies, the simulation results generally agreed well with the experimental results. In other words, the numerical model can rationally reflect the impact load performance of RC and SFRC slabs.

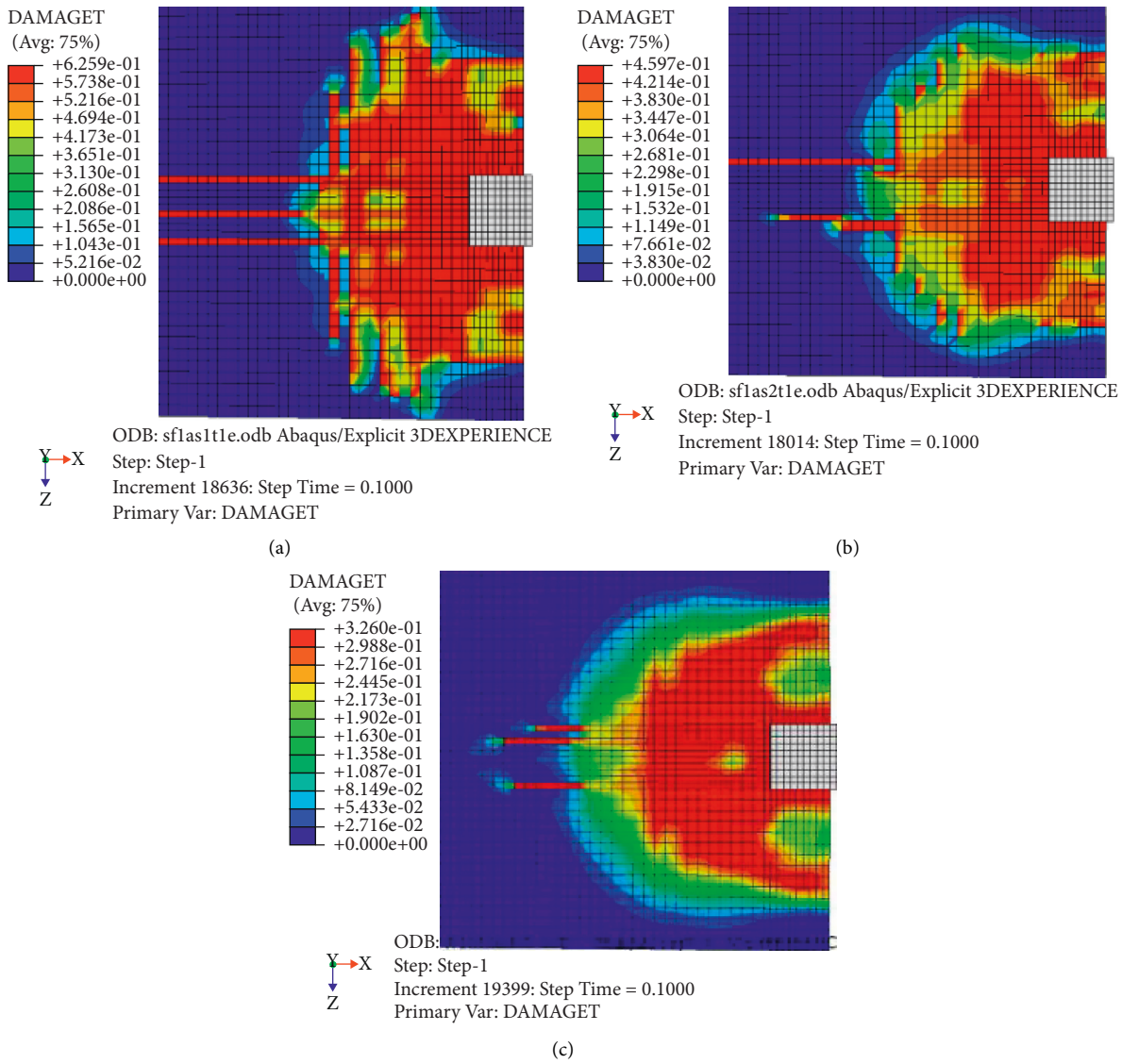

Figure 12: Tension damage of SF1-E specimens for aspect ratio of (a) as = 45, (b) as = 65, and (c) as = 80.

3. Results and Discussion

Verified FE models were employed herein to perform a comprehensive parametric study in order to investigate the effects of the different load and structure-related parameters on the response of plain concrete and steel-fiber-reinforced concrete slab-on-grade under impact loading. The main parameters investigated in this study are the volume fraction of steel fiber added in concrete, aspect ratio of steel fiber, thickness of slab, impact mass and velocity, and location of load (i.e., edge, interior, and corner). The behavior was assessed by monitoring the displacement and failure mode. A total of 108 models are simulated.

3.1. Effect of Fiber Aspect Ratio. The impact load capacity and displacement of SFRC specimens containing different fractions of fiber by volume, each fraction with different aspect ratios of fiber, were analyzed for the three loading positions (i.e., interior, edge and corner) and the results were shown in Figures 6–8. The maximum increase was obtained for concrete with a aspect ratio of 80 at a fiber volume fraction of 1.5% for all loading positions. It can be observed in general from the figures that for a particular fiber mix proportion, the best performance in displacement, as well as failure impact resistance of the steel fibrous concrete, is given by concrete containing fiber volume of 0.5%, 1%, and 1.5% for aspect ratio of 80.

The increase in impact resistance can be seen from the reduced slab deflection after the impact load was applied on the slab the peak displacement varied for each fiber percentage and aspect ratio. The maximum increase was observed for fibrous concrete with an aspect ratio of 80 concrete containing 1.5% volume fractions of fispec.

As it can be seen from Figure 9 for an aspect ratio of 45, the slab deflection is almost the same as plain concrete slab deflection for all loading positions. This implies that small fibers are least effective in arresting cracks caused by impact

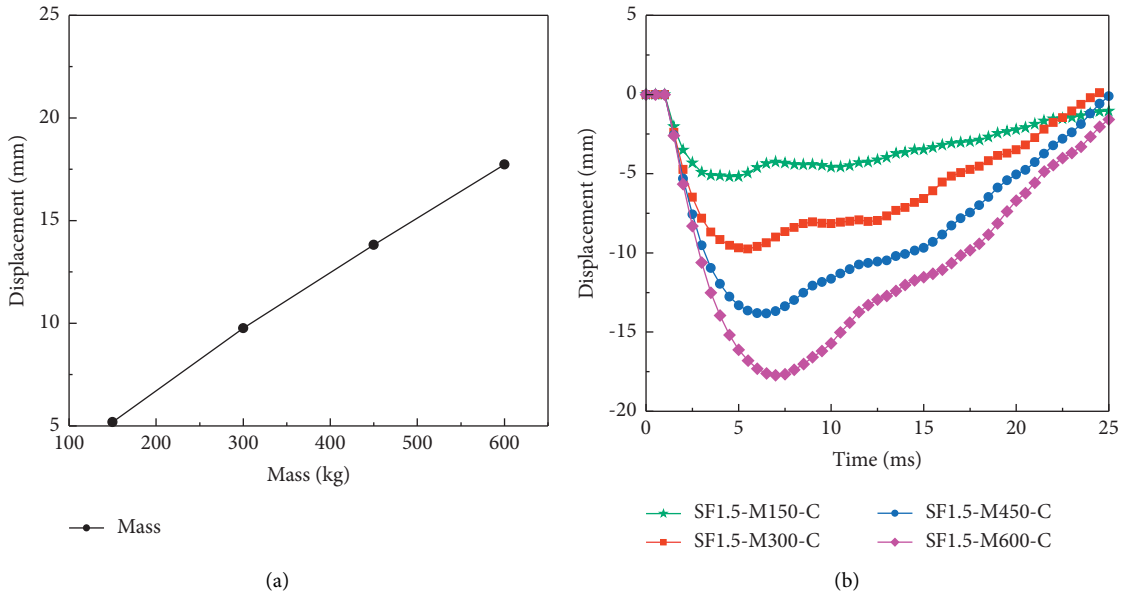

Figure 13: (a) Peak displacement mass graph of specimen II models for center load, (b) deflection time history of specimen II models for center load.

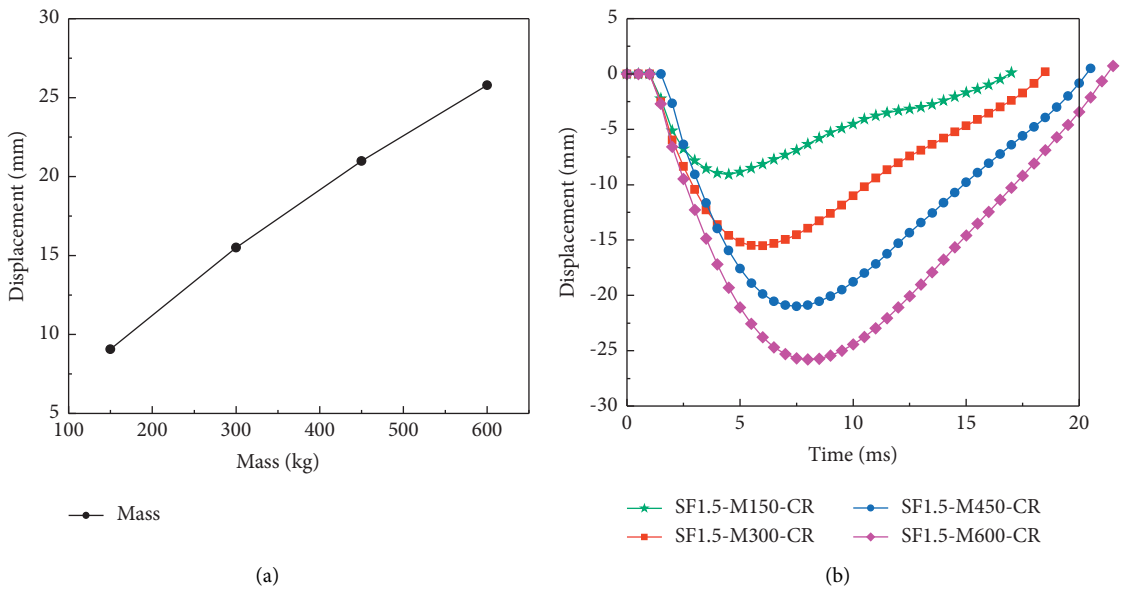

Figure 14: (a) Peak displacement velocity graph of specimen III models for corner load, (b) deflection time history of specimen II models for corner load.

loading, which may be due to small bonding stress with concrete and thus get pulled out of the matrix easily. Relatively longer fibers are most effective in arresting the cracks due to impact loading because of their higher bond resistance.

In general, it can be concluded that on increasing aspect ratios and with the increase in fiber content, the impact resistance increases. Furthermore, it can also be concluded that the incorporation of steel fiber in plain concrete has significantly improved the impact resistance of concrete.

As observed from the damages for the three loading locations in Figures 10–12, the progression of damage decreases as the aspect ratio increases. The maximum reduction in the intensity of damage was obtained for concrete with an aspect ratio of 80 at a fiber volume fraction of 1.5%. It can be concluded from the result that as the aspect ratio decreased, there is a decrease in the performance of fibrous concrete against impact loading. It seems that small fiber is least effective in arresting the cracks created due to impact loading, their small length offers less bond resistance, and smaller fibers are pulled out of the matrix. Longer fibers are most effective in arresting the cracks due to impact loading because of their higher bond resistance.

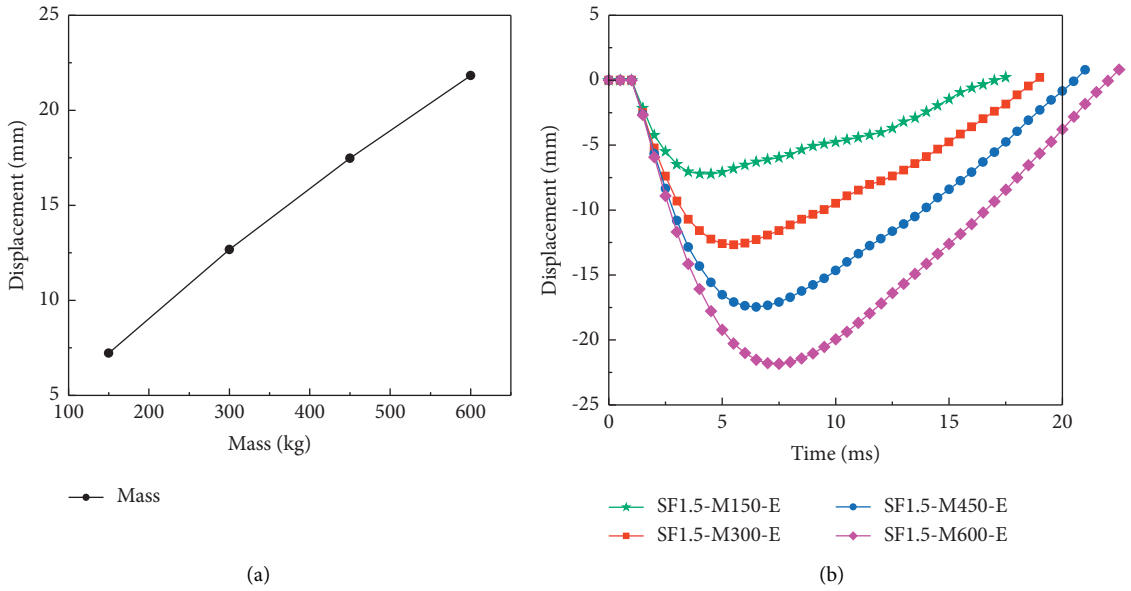

Figure 15: (a) Peak displacement velocity graph of specimen II models for edge load, (b) deflection time history of specimen II models for edge load.

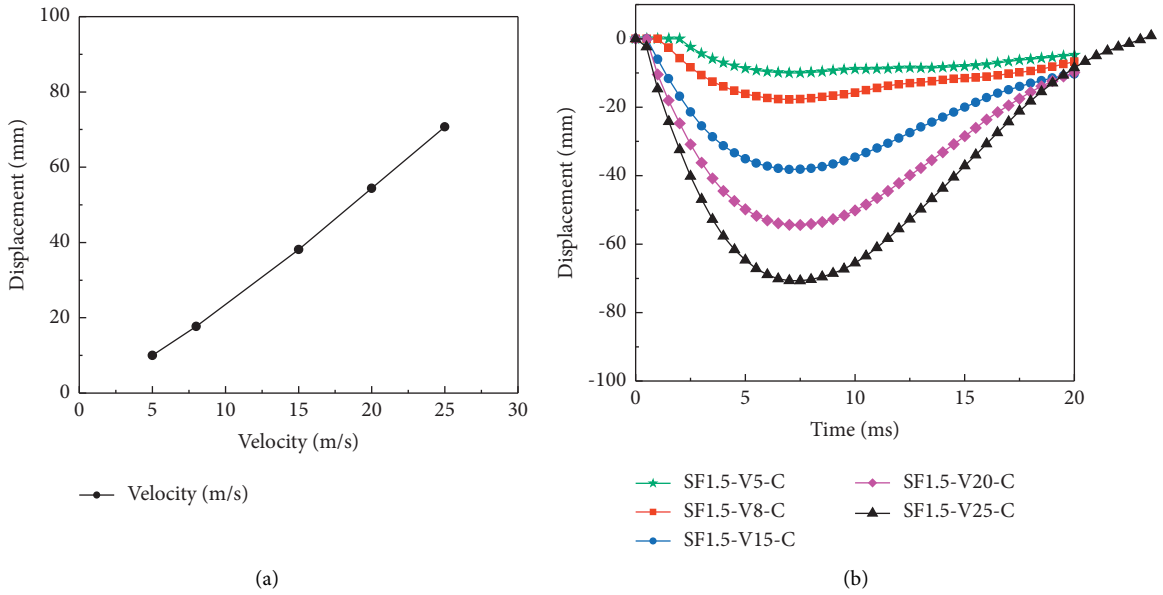

Figure 16: (a) Peak displacement velocity graph of specimen III models for center load, (b) deflection time history of specimen III models for center load.

3.2. Effect of Impact Mass. The impact mass of the drop head impactor was selected as 150 kg, 300 kg, 450 kg, and 600 kg, so that it could develop enough deflection on the top surface of the concrete slab. A constant impact velocity of 8 m/s was selected to study the effect of the impact mass on deflection since reasonable deflection was found from the impact test for a specimen similar to the FE model at this velocity, so this impact velocity was considered. Figures 13–15 show the variation of the deflection with different impact masses for the three loading locations.

The figures show that the deflection of the slab was increased nonlinearly with the increase of the mass of the impactor. The increase of mass increased the impact energy and thereby increased the deflection of the concrete slab. In summary, the impact mass was found as a significant parameter in increasing the deflection of the concrete slab.

For steel-fiber-reinforced concrete, the impact resistance is higher for larger impact mass as the damage increases, and the impact resistances increase for a higher percentage of steel-fiber-reinforced concrete.

3.3. Effect of Impact Velocity. The impact velocity of the impactor was selected as 5 m/s, 8 m/s, 15 m/s, 20 m/s, and

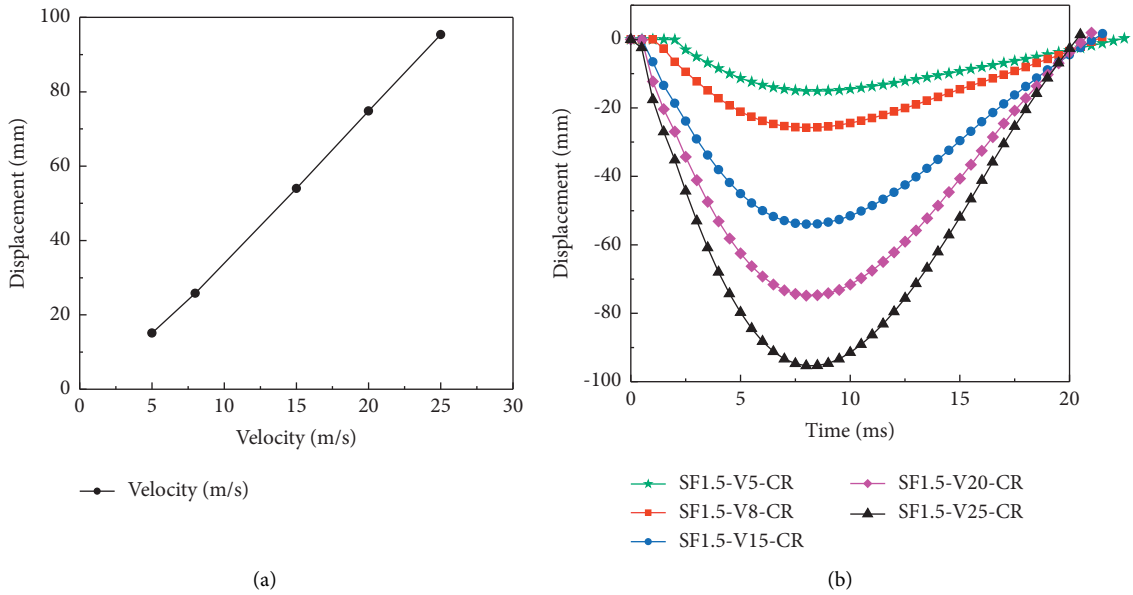

Figure 17: (a) Peak displacement-velocity graph of specimen III models for corner load, (b) deflection time history of specimen III models for corner loading.

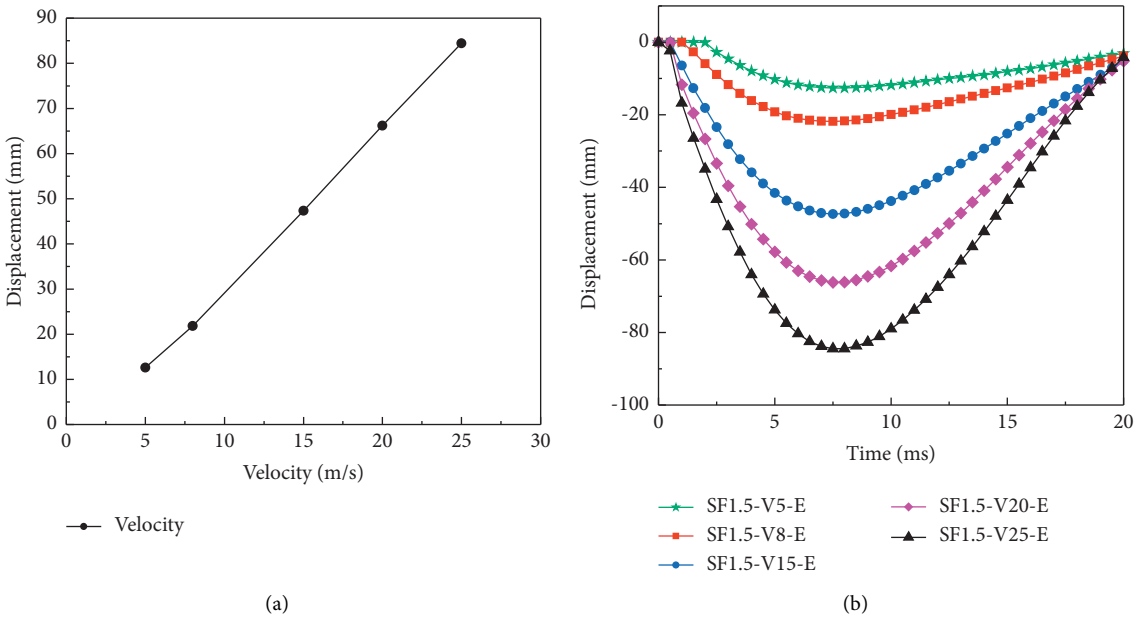

Figure 18: (a) Peak displacement-velocity graph of specimen III models for edge load, (b) deflection time history of specimen III models for edge loading.

25 m/s for a concrete slab with a constant impact mass of 600 kg to investigate the influence of impact velocity on the deflection of a concrete slab under impact load. A constant impact mass of 600 kg implies that for the different impact velocities of the impactor, the mass of the impactor was the same. The impactor was a 300 mm rectangle with a height of 25 mm. The sides of the impactor were 300 mm, and the thickness was 25 mm. The mass of the impactor was 600 kg. Figures 16–18 show the variation of deflection with different impact velocities.

The above figures show that the deflection of concrete slab was increased slightly nonlinearly with the increase of impact velocity within the selected range. The five values of impact velocities were selected as the range was found suitable to produce significant deflection. It was found that the selection of a value smaller than the lowest value of the range could not develop significant deflection whereas a value larger than the highest value of the range could damage the selected specimen. The initial slope of the deflection versus impact velocity graph was steeper compared to the

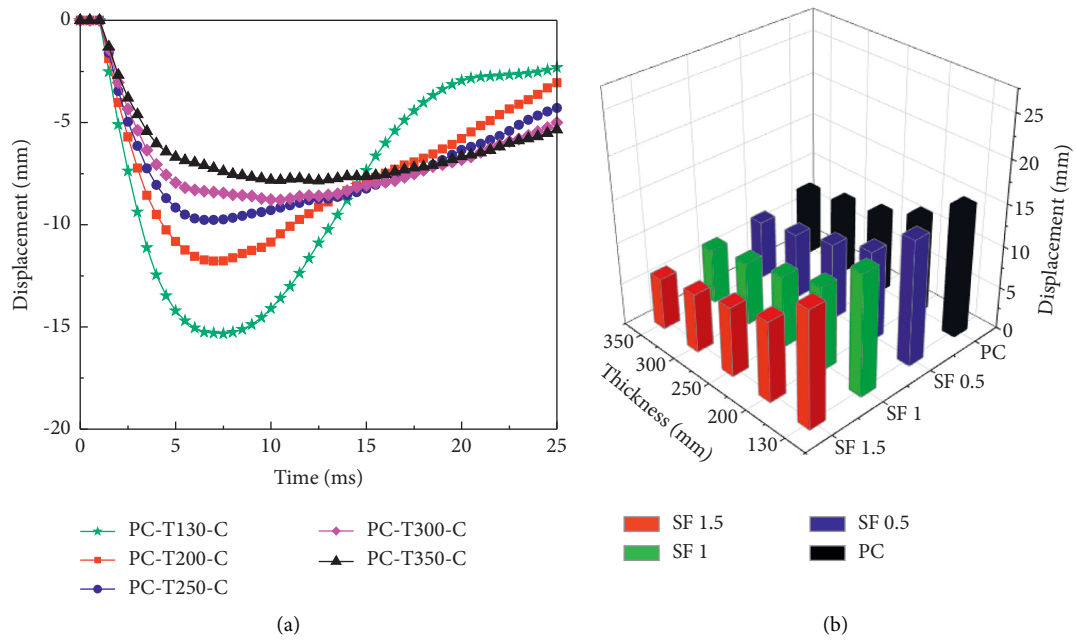

Figure 19: (a) Displacement time history curve for PC-T-C, (b) peak displacement for combined thickness and V_f percentage variations.

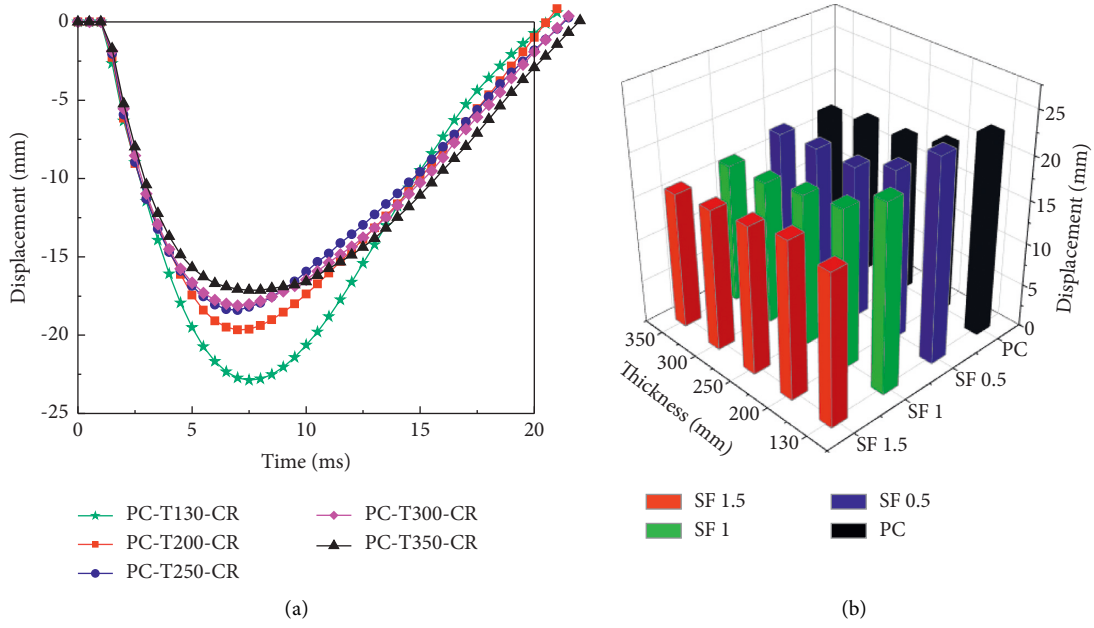

Figure 20: (a) Displacement time history of specimen PC-T-CR, (b) peak displacement for combined thickness and V_f percentage variations.

next slope which implies that the effect of impact velocity in controlling deflection was reduced with the further increase of impact velocity.

As the impact velocity increases, the deflection increases. Projectile mass increases the kinetic energy, which increases the penetration depth, but the increase ratio is reduced at a certain level. Thus, although both the impact velocity and projectile mass increase the impact energy, the impact damage of the concrete target is more vulnerable to the high-velocity impact than the heavy-mass impact. A large projectile diameter increases the resisting area of the concrete target, which decreases the penetration depth.

3.4. Thickness of Slab. Different thicknesses of the concrete slab were selected at 130, 200, 250, 300, and 350 mm to study the significance of slab thickness on varying the deflection of a concrete slab under impact loading. Figures 19–21 indicate the variation of the deflection of the concrete slab with different thicknesses of the concrete slab.

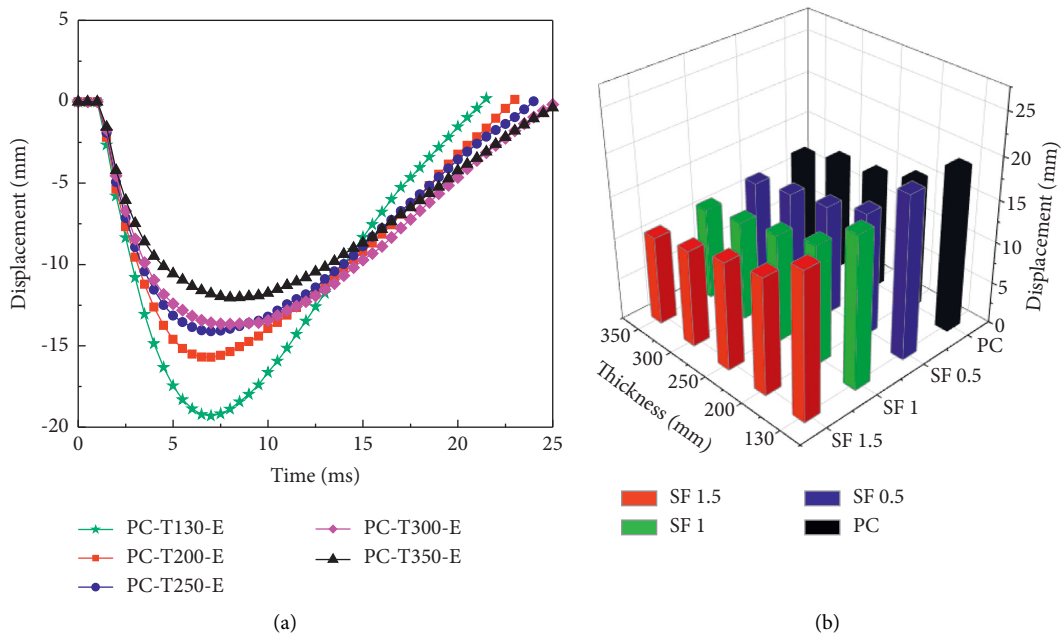

(a) (b)

Figure 21: (a) Displacement time history response of PC-T-E, (b) peak displacement due to thickness and V_f variation for edge loading.

The deflection of the concrete slab for all loading position cases decreases with the increase of slab thickness within the selected values as shown in Figures. Thereby the slab thickness is also expected to influence the deflection significantly under impact loads.

4. Conclusions

In this study, the behavior of plain concrete and SFRC slab-on-grade has been investigated. An extensive parametric study has been carried out to investigate the effectiveness of the steel fiber volume fraction content added to concrete for increasing the impact resistance of slab-on-grade and the influence of different aspect ratios of fiber along with different fiber volume percentages on the response of SFRC slab-on-grade under impact loading. The displacement time history, modes of failure, and energy dissipation capacity responses are monitored. The following conclusions can be drawn.

(i) From damages and crack patterns, the steel fiber contributed to decreasing the intensity of damage and crack progression. The effective use of steel fiber volume in concrete along with a large aspect ratio significantly improved the impact resistance of the slab-on-grade by reducing the deflection and reducing the intensity of damage and crack. The results revealed that the addition of 0.5%, 1%, and 1.5% volume fractions of steel fiber in concrete could reduce up to 5%, 8%, and 25% of deflection of the slab, respectively. The maximum increase of 11%, 26%, and 11% was observed for fibrous concrete with an aspect ratio of 80 concrete containing 1.5% volume fractions of fibers for loading at center, corner, and edge, respectively.

(ii) It can be concluded from the result that as the aspect ratio decreased, there is a decrease in the performance of fibrous concrete against impact loading. This indicates that small fibers are least effective in arresting the cracks induced due to impact loading, may be due to their small length, they offer less bond and are pulled out of the matrix easily.

(iii) The use of steel fibers increases the flexural tensile strength of concrete, which decreases the penetration depth. The use of steel fiber with 1.5% volume ratio decreases about 25% of the concrete target thickness.

Data Availability

The data are available upon request from the corresponding author.

Conflicts of Interest

The authors declare that there are no conflicts of interest regarding the publication of this paper.

Acknowledgments

This research was partially supported by the Addis Ababa Science and Technology University as a partial fulfillment for MSc degree in Civil Engineering.

References

[1] A. Vaitkus, J. Grazulyte, and R. Kleiziene, "Influence of static and impact load on pavement performance," in *Proceedings of the International Conference on Environmental Engineering. ICEE*, 2014.

[2] A. Ali and M. Mohod, "A review on effect of fiber reinforced concrete on rigid pavement," *Int. J. Res. Eng. Sci. Technol*, vol. 1, pp. 222–227, 2015.

[3] S. Ali, "Performance of protective composite runway pavement under moving and impact loads," Doctoral dissertation, Queensland University of Technology, Australia, 2018.

[4] S. Ali, S. Fawzia, D. Thambiratnam, X. Liu, and A. M. Remennikov, "Performance of protective concrete runway pavement under aircraft impact loading," *Structure and Infrastructure Engineering*, vol. 16, no. 12, pp. 1698–1710, 2020.

[5] S. Ali, X. Liu, and S. Fawzia, "Numerical study on the surface depression of the concrete runway pavement under impact load," *International Journal of Research in Civil Engineering, Architecture and Design (IJRCEAD)*, vol. 4, no. 1, pp. 8–19, 2016.

[6] S. N. Shoukry, D. R. Martinelli, and O. I. Selezneva, "Dynamic performance of composite pavements under impact," *Transportation Research Record: Journal of the Transportation Research Board*, vol. 1570, no. 1, pp. 163–171, 1997.

[7] T. K. Erdem, S. Demirhan, G. Yıldırım et al., "Effects of mixture design parameters on the mechanical behavior of high-performance fiber-reinforced concretes," *Journal of Materials in Civil Engineering*, vol. 32, no. 12, Article ID 04020368, 2020.

[8] V. Ramakrishnan, G. Y. Wu, and G. Hosalli, "Flexural fatigue strength, endurance limit and impact strength of fiber reinforced concretes," *Transportation Research Record*, vol. 1226, pp. 17–24, 1989.

[9] G. Yıldırım, "Dimensional stability of deflection-hardening hybrid fiber reinforced concretes with coarse aggregate: suppressing restrained shrinkage cracking," *Structural Concrete*, vol. 20, no. 2, pp. 836–850, 2019.

[10] Q. S. Banyhussan, G. Yıldırım, Ö. Anıl, R. T. Erdem, A. Ashour, and M. Şahmaran, "Impact resistance of deflection-hardening fiber reinforced concretes with different mixture parameters," *Structural Concrete*, vol. 20, no. 3, pp. 1036–1050, 2019.

[11] P. Behinaein, A. A. Abbas, and D. M. Cotsovos, "FE modelling of SFRC beams under impact loads," in *Proceedings of the 7th European Congress on Computational Methods in Applied Sciences and Engineering*, 2016.

[12] S. Demirhan, G. Yıldırım, Q. S. Banyhussan et al., "Impact behaviour of nanomodified deflection-hardening fibre-reinforced concretes," *Magazine of Concrete Research*, vol. 72, no. 17, pp. 865–887, 2020.

[13] L. Jin, R. Zhang, L. Li, X. Du, and Y. Yao, "Impact behavior of SFRC beams at elevated temperatures: experimental and analytical studies," *Engineering Structures*, vol. 197, Article ID 109401, 2019.

[14] M. Papadrakakis, V. Papadopoulos, G. Stefanou, and V. Plevris, "FE modelling of SFRC beams under impact loads," in *Proceedings of the European congress on computational methods in applied sciences and engineering*, 2016.

[15] G. Ulzurrun and C. Zanuy, "Flexural response of SFRC under impact loading," *Construction and Building Materials*, vol. 134, pp. 397–411, 2017.

[16] Ş. Yazıcı, H. Ş. Arel, and V. Tabak, "The effects of impact loading on the mechanical properties of the SFRCs," *Construction and Building Materials*, vol. 41, pp. 68–72, 2013.

[17] G. Yıldırım, F. E. Khiavi, Ö. Anıl, O. Şahin, M. Şahmaran, and R. T. Erdem, "Performance of engineered cementitious composites under drop-weight impact: effect of different mixture parameters," *Structural Concrete*, vol. 21, no. 3, pp. 1051–1070, 2020.

[18] S. Choudhary, A. Jain, H. Bhavsar, S. Chaudhary, and R. Choudhary, "Analysis of steel fiber reinforced concrete wall panels under compression, flexural and impact loading," *Materials Today Proceedings*, vol. 38, pp. 2471–2475, 2021.

[19] J. A. O. Barros and J. A. Figueiras, "Model for the analysis of steel fibre reinforced concrete slabs on grade," *Computers & Structures*, vol. 79, no. 1, pp. 97–106, 2001.

[20] B. Belletti, R. Cerioni, A. Meda, and G. Plizzari, "Experimental and numerical analyses of FRC slabs on grade," in *Proceedings of the FRAMCOS5 Conference*, Vail Colorado, 2004.

[21] B. Belletti, R. Cerioni, A. Meda, and G. Plizzari, "Design aspects on steel fiber-reinforced concrete pavements," *Journal of Materials in Civil Engineering*, vol. 20, no. 9, pp. 599–607, 2008.

[22] S. Chen, "Strength of steel fibre reinforced concrete ground slabs," *Proceedings of the Institution of Civil Engineers - Structures and Buildings*, vol. 157, no. 2, pp. 157–163, 2004.

[23] S. Chen, "Steel fiber concrete slabs on ground: a structural matter," *ACI Structural Journal*, vol. 104, no. 3, p. 373, 2007.

[24] X. Dong and J. Gao, "Effects of fiber type and fiber volume content on frost resistance of fiber-reinforced concrete in airport pavement," *ICTE*, vol. 2011, pp. 1524–1529, 2011.

[25] K. Jain, M. Singh, and P. Singh, *Steel Fibre Reinforced Concrete and Pavements: A Review*, 2015.

[26] C. Lee, S. Lee, K. Ko, and J.-M. Yang, "Structural performance of SFRC slab-on-grade supported on elastic spring system," *Magazine of Concrete Research*, vol. 69, no. 15, pp. 757–771, 2017.

[27] A. Meda, G. A. Plizzari, and P. Riva, "Fracture behavior of SFRC slabs on grade," *Materials and Structures*, vol. 37, no. 6, pp. 405–411, 2004.

[28] A. Meda, G. A. Plizzari, L. Sorelli, and B. Rossi, *Fracture Mechanics for SFRC Pavement. Concrete Structures: The Challenge of Creativity*, 2003.

[29] P. Overlays, A. Brand, S. Shields-Cook, and D. Harrington, *Fiber-Reinforced Concrete for Pavement Overlays*, 2019.

[30] J. Roesler, A. Bordelon, A. S. Brand, and A. Amirkhanian, *Fiber-Reinforced Concrete for Pavement Overlays: Technical Overview*, 2019.

[31] L. G. Sorelli, A. Meda, and G. A. Plizzari, "Steel fiber concrete slabs on ground: a structural matter," *ACI Materials Journal*, vol. 103, no. 4, p. 551, 2006.

[32] A. S. U. S. Manual, "Abaqus," vol. 6, 2012, http://130.149.89.49:2080/v6.14/.

[33] A. U. Manual, *Abaqus User Manual*, Abacus, 2020.

[34] A. Simulia, *6.19, ABAQUS Anal. Theory Manuals, SIMULIA, Dassault Systèmes, Realis. Simulation*, Rhode Island RI, USA, 2019.

[35] P. Wriggers and T. A. Laursen, *Computational Contact Mechanics*, vol. 2, Springer, Berlin, Germany, 2006.

[36] E. Hognestad, *Study of Combined Bending and Axial Load in Reinforced concrete Members*, 1951.

[37] P.-E. Petersson, *Crack Growth and Development of Fracture Zones in plain concrete and Similar Materials*, Lund University, Lund, Sweden, 1981.

[38] S.-C. Lee, J.-H. Oh, and J.-Y. Cho, "Compressive behavior of fiber-reinforced concrete with end-hooked steel fibers," *Materials*, vol. 8, no. 4, pp. 1442–1458, 2015.

[39] F. Bencardino, L. Rizzuti, G. Spadea, and R. N. Swamy, "Stress-strain behavior of steel fiber-reinforced concrete in compression," *Journal of Materials in Civil Engineering*, vol. 20, no. 3, pp. 255–263, 2008.

[40] A. S. Ezeldin and P. N. Balaguru, "Normal-and high-strength fiber-reinforced concrete under compression," *Journal of Materials in Civil Engineering*, vol. 4, no. 4, pp. 415–429, 1992.
[41] L. S. Hsu and C. T. Hsu, "Stress-strain behavior of steel-fiber high-strength concrete under compression," *Structural Journal*, vol. 91, no. 4, pp. 448–457, 1994.
[42] M. A. Mansur, M. S. Chin, and T. H. Wee, "Stress-strain relationship of high-strength fiber concrete in compression," *Journal of Materials in Civil Engineering*, vol. 11, no. 1, pp. 21–29, 1999.
[43] M. Nataraja, N. Dhang, and A. Gupta, "Stress–strain curves for steel-fiber reinforced concrete under compression," *Cement and Concrete Composites*, vol. 21, no. 5-6, pp. 383–390, 1999.
[44] L. Á. d. Oliveira Júnior, V. E. d. S. Borges, A. R. Danin et al., "Stress-strain curves for steel fiber-reinforced concrete in compression," *Matèria. Revista Internacional d'Art*, vol. 15, no. 2, pp. 260–266, 2010.
[45] X. Shi, P. Park, Y. Rew, K. Huang, and C. Sim, "Constitutive behaviors of steel fiber reinforced concrete under uniaxial compression and tension," *Construction and Building Materials*, vol. 233, Article ID 117316, 2020.
[46] T. S. Lok and J. R. Xiao, "Flexural strength assessment of steel fiber reinforced concrete," *Journal of Materials in Civil Engineering*, vol. 11, no. 3, pp. 188–196, 1999.
[47] J. A. O. Barros and J. A. Figueiras, "Flexural behavior of SFRC: testing and modeling," *Journal of Materials in Civil Engineering*, vol. 11, no. 4, pp. 331–339, 1999.
[48] B. Li, Y. Chi, L. Xu, C. Li, and Y. Shi, "Cyclic tensile behavior of SFRC: experimental research and analytical model," *Construction and Building Materials*, vol. 190, pp. 1236–1250, 2018.
[49] T. S. Lok and J. R. Xiao, "Tensile behaviour and moment-curvature relationship of steel fibre reinforced concrete," *Magazine of Concrete Research*, vol. 50, no. 4, pp. 359–368, 1998.
[50] G. Meng, B. Wu, S. Xu, and J. Huang, "Modelling and experimental validation of flexural tensile properties of steel fiber reinforced concrete," *Construction and Building Materials*, vol. 273, Article ID 121974, 2021.
[51] Y. Meng, H. Chengkui, and W. Jizhong, "Characteristics of stress-strain curve of high strength steel fiber reinforced concrete under uniaxial tension," *Journal of Wuhan University of Technology-Materials Science Edition*, vol. 21, no. 3, pp. 132–137, 2006.
[52] W. G. Davids, "Foundation modeling for jointed concrete pavements," *Transportation Research Record: Journal of the Transportation Research Board*, vol. 1730, no. 1, pp. 34–42, 2000.
[53] A. Ioannides and J. Donnelly, *Three-dimensional Analysis of Slab on Stress-dependent Foundation*, 1988.
[54] L. Taerwe and S. Matthys, *Fib Model Code for concrete Structures 2010*, Ernst & Sohn, Wiley, New York, NY, USA, 2013.
[55] L. J. Malvar and J. E. Crawford, *Dynamic Increase Factors for concrete*, 1998.
[56] L. Yang, X. Lin, and R. J. Gravina, "Evaluation of dynamic increase factor models for steel fibre reinforced concrete," *Construction and Building Materials*, vol. 190, pp. 632–644, 2018.
[57] T. D. Hrynyk and F. J. Vecchio, "Modeling of reinforced and fiber-reinforced concrete slabs under impact loads," *ACI Structural Journal*, vol. 321, pp. 8–20, 2017.
[58] Y. Sümer and M. Aktaş, "Defining parameters for concrete damage plasticity model," *Challenge Journal of Structural Mechanics*, vol. 1, no. 3, pp. 149–155, 2015.
[59] H. Behnam, J. S. Kuang, G. Spadea, and B. Samali, "Parametric finite element analysis of RC wide beam-column connections," *Computers & Structures*, vol. 205, no. 3, pp. 28–44, 2018.